Conference on Modelling Fluid Flow (CMFF'25)
The 19th International Conference on Fluid Flow Technologies
Budapest, Hungary, August 26 - August 29, 2025

PREDICTIONS OF PARTICLE TRAJECTORY RESPONSE TO REYNOLDS NUMBER IN TURBULENT CHANNEL FLOWS USING ARTIFICIAL NEURAL NETWORKS

Lee MORTIMER[1], Michael FAIRWEATHER[2]

[1] Corresponding Author. School of Chemical and Process Engineering, Faculty of Engineering and Physical Sciences, University of Leeds. Leeds LS2 9JT, United Kingdom. E-mail: l.f.mortimer@leeds.ac.uk
[2] School of Chemical and Process Engineering, Faculty of Engineering and Physical Sciences, University of Leeds. Leeds LS2 9JT, United Kingdom. E-mail: m.fairweather@leeds.ac.uk

ABSTRACT

The present work details the development, implementation and performance of a machine-learning (ML) based predictive model for simulating particle-laden wall-bounded turbulent flows. Additionally, the technique is demonstrated with a particular focus on investigating the influence of Reynolds number on particle trajectory responses, comparing with equivalent high-fidelity simulations. Using a hybrid ML algorithm, the model is trained using data from direct numerical simulation (DNS) and Lagrangian particle tracking (LPT) in turbulent channel flows. Training trajectories are obtained from $Re_\tau = 180$ and $Re_\tau = 300$ DNS-LPT predictions across multiple particle Stokes numbers, however, the value of the technique is demonstrated at intermediate Reynolds numbers ($Re_\tau = 240$), which offers strong agreement with DNS-LPT obtained first- and second-order velocity statistics, emphasising the accuracy at predicting particle dynamics at Reynolds numbers the ML model was never trained on. The techniques' effectiveness demonstrates the ability to minimise the need for extensive DNS-LPT particle trajectory data which maintaining high accuracy in predicting dynamic properties and emergent phenomena across different Reynolds numbers. Beyond its immediate scope, this approach has broad applications in industrial and environmental processes where predictive models for turbulent multiphase flows are critical, such as aerosol transport and nuclear waste processing.

Keywords: machine learning, artificial neural networks, direct numerical simulation, Lagrangian particle tracking, turbulent particle-laden channel flows, Reynolds number

NOMENCLATURE

C_D	[-]	drag coefficient
I	[-]	training input vector
N	[-]	spectral element method (SEM) order
N_P	[#]	number of simulated particles
Re_B	[-]	bulk Reynolds number
Re_τ	[-]	shear Reynolds number
U_B	[ms^{-1}]	bulk velocity
d_P^*	[-]	particle diameter
$\boldsymbol{f}^*$	[-]	forcing function
p^*	[-]	pressure field
t^*	[-]	time
u_τ	[ms^{-1}]	fluid shear velocity
$\boldsymbol{u}_F^*$	[-]	fluid velocity vector
u'^*_F	[-]	fluid velocity fluctuation
$\boldsymbol{u}_P^*$	[-]	particle velocity vector
$\boldsymbol{u}_S^*$	[-]	slip velocity vector
$\boldsymbol{x}^*$	[-]	position vector
δ	[m]	channel half-height
ν_F	[m^{2}s^{-1}]	fluid kinematic viscosity
ρ_F	[kgm^{-3}]	fluid density
ρ_P^*	[-]	particle-fluid density ratio
Δt^*	[-]	DNS timestep

Subscripts and Superscripts

P, F	particle, fluid
B, τ	bulk, shear
$*$	bulk non-dimensional units
RMS	root mean square

1. INTRODUCTION

Machine learning (ML) has emerged in recent years as a vital tool in enhancing analysis, research, predictive capabilities and decision-making across countless applications [1]. In essence, the term ML itself encompasses a wide variety of algorithms and

modelling tools used originally for data analysis, but which have been adopted across many scientific disciplines over the last few decades [2]. In such scenarios, ML applications have grown significantly. For instance, in healthcare, ML is capable of diagnosing and predicting diseases through analysis of medical data and imaging [3]. Its scope extends beyond that of scientific purposes into industries such as finance and automation of vehicles where it supports fraud detection [4] and navigation and decision-making in self-driving cars [5]. In such applications, the ability for ML to 'learn' is grounded in being able to obtain training data, from which insights and information can be extracted to develop intelligent models.

Applications of ML further extend into the field of fluid dynamics, facilitated by the existence (and generation) of extensive data from both computational simulations and experiments. ML has been used to address challenges such as turbulence closure models, reduced-order modelling [6] and flow optimisation and control [7, 8]. Jain et al. [9] applied random forest regression in order to predict fluid flow in curved pipes using simulation-generated training data. Aside from mispredictions of vortex positions, the technique was shown to accurately capture important characteristics of turbulent flow in non-trivial geometries. Li et al. [10] used k-nearest neighbour (KNN) techniques to learn the features of mixing tank systems obtained from limited experimental Lagrangian trajectories, demonstrating the effectiveness of ML algorithms applied in the context of experimentally obtained datasets. Yang et al. [11] expanded upon this by introducing the concept of a 'hybrid' ML model which combined preprocessors, noise generators and particle-wall collision algorithms to simulate turbulent single-phase and particle-liquid flows in pipes. This approach was shown to accurately predict local fluid and particle velocities, as well as spatial concentration distributions, having been trained on solely dynamic experimental data.

As the complexity of the fluid dynamic system increases, due to the presence of complex geometries or additional phases, investigation into such scenarios poses greater challenges due to the intricacies of the additional interactions involved. In such systems, the fluid velocity field may fluctuate both due to the existence of turbulent eddies, as well as two-way coupling between particulate phases and the continuous flow field [12] which influences turbulence modulation, and four-way coupling wherein particles may interact with other particles via collision or agglomeration [13]. Being able to capture these phenomena in lower fidelity simulation techniques stands as an ongoing challenge in computational fluid dynamics, which for most purposes one must turn to high fidelity methods such as direct numerical simulation (DNS) and immersed boundary methods to holistically represent the system and extract knowledge from fully resolved simulations. These are often very computationally intensive and require high timeframes to perform the computations. The elucidation of such processes using high fidelity techniques is hence crucial for increasing the accuracy at which these processes are represented in lower order models, which in turn is vital for industrial applications such as the development of digital twins [14].

The present study aims to develop and demonstrate an enhanced predictive model which uses a hybrid ML approach to determine key fluid and particle behaviour in turbulent flows. An artificial neural network (ANN) is trained on dynamic particle databases generated from DNS and Lagrangian particle tracking (LPT) in channel flows. The model seeks to replicate similar trajectories and hence bulk flow observations such as velocity profiles of both phases and concentration profiles of the particulate phase, while reducing the amount of computational resources and time necessary to obtain similar degrees of accuracy. The study further aims to demonstrate the generalisability of the technique, applying the trained algorithm to parameter sets outside those trained upon, in this case considering a Reynolds number previously unseen by the ML algorithm. Finally, the technique builds upon previous attempts [11] by incorporation lagged particle velocities into the training input, manifesting the concept of particle momentum within the model, further generalising the technique to high Stokes number regimes, wherein particle motion is more decorrelated from the local fluid streamlines.

2. METHODOLOGY

2.1. Direct Numerical Simulation

To obtain high accuracy predictions of the continuous flow field capable of capturing all relevant turbulence length and timescales, the DNS code Nek5000 [15] was employed in the context of a turbulent channel flow at various shear Reynolds numbers, $Re_\tau = u_\tau \delta / \nu_F = 180, 240$ and 300. Here, u_τ is the shear velocity, δ is the channel half-height and ν_F is the kinematic viscosity of the fluid phase. Nek5000 uses a spectral element method-based Eulerian solver at high order ($N = 7$) to model the temporal and spatial evolution of the flow field, and is applied on a hexahedral spectral element grid representing a standard channel flow geometry.

The governing equations for the continuous phase are the Navier-Stokes (NS) equations, expressed in non-dimensional form using bulk flow properties to achieve the following:

$$\nabla \cdot \boldsymbol{u}_F^* = 0, \tag{1}$$

$$\frac{D\boldsymbol{u}_F^*}{Dt^*} = -\nabla p^* + \frac{1}{Re_B}\nabla^2 \boldsymbol{u}_F^* + \boldsymbol{f}_{PG}^* + \boldsymbol{f}_{2W}^*. \tag{2}$$

Here, $\boldsymbol{u}_F^*(\boldsymbol{x}^*, t^*)$ represents the fluid velocity vector at position $\boldsymbol{x}^*$ and time t^*, while $p^*(\boldsymbol{x}^*, t^*)$ is the fluid pressure, $Re_B = u_B\delta/\nu_F$ is the bulk Reynolds number, $\boldsymbol{f}_{PG}^*$ is a constant pressure gradient forcing term and $\boldsymbol{f}_{2W}^*$ is an arbitrary cell-dependent forcing term which accounts for two-way momentum exchange between particles and fluid (two-way coupling). In the above and subsequent equations, parameters which are marked with an asterisk $(*)$ imply non-dimensional variables achieved using bulk properties, $(\delta,\ U_B,\ \rho_F)$, with ρ_F the fluid density.

The NS equations are solved numerically on a structured Cartesian grid composed of 27 × 18 × 23 spectral elements of 7th order, amounting to approximately 3.9 million equivalent 'nodes'. The grid is refined in the wall-normal direction to capture near-wall flow structures more accurately, while a uniform distribution of elements is maintained in the streamwise and spanwise directions. The computational domain, defined as $12\delta\times2\delta\times6\delta$, represents a channel geometry. These dimensions are selected to capture all significant vortical structures, and the geometry is illustrated in Fig. 1.

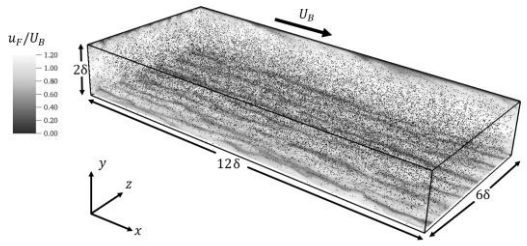

Figure 1: Schematic of the particle-laden turbulent channel flow at Re_τ =180 used in DNS-LPT simulations

The solver uses a constant time step of $\Delta t^* = 0.005$. Periodic conditions are imposed in the streamwise and spanwise directions to ensure that the flow remains cyclic. The extents of the wall-normal direction are located at $y^* = \pm1$ and are subject to no-slip and impermeability conditions. The flow is driven by a constant pressure gradient applied in the streamwise (x^*) direction, with the pressure gradient magnitude specified as follows:

$$\frac{dp^*}{dx^*} = \left(\frac{Re_\tau}{Re_B}\right)^2. \tag{3}$$

2.2. Lagrangian Particle Tracking

To track the trajectories of solid particles within the flow, a Lagrangian particle tracking routine was developed and integrated to run concurrently with the fluid phase solver within Nek5000. Each particle is modelled as a point-like, rigid, impenetrable computational sphere. After each time step of the continuous phase completes, the LPT routine solves the non-dimensional equations of motion for each particle considering a force-balance which acts on the particle's inertia, as described by Maxey [16] and Patterson and Riley [17]. A key objective in developing the hybrid ML algorithm is to generalise the model across a range of Stokes numbers. As a result, forces such as lift, virtual mass, and pressure gradient, in addition to drag, are considered in the calculations since they may be significant under certain conditions, as noted in previous studies [18]. However, the Basset history force is excluded due to its high computational cost and earlier findings suggesting its negligible effect on particle motion [19]. The Newtonian equations governing each particle's motion are as follows:

$$\frac{d\boldsymbol{x}_P^*}{dt^*} = \boldsymbol{u}_P^*, \tag{4}$$

$$\begin{aligned}\mathrm{M_{VM}}\frac{\partial \boldsymbol{u}_P^*}{\partial t^*} = &\underbrace{\frac{3C_D|\boldsymbol{u}_S^*|}{4d_p^*\rho_P^*}\boldsymbol{u}_S^*}_{Drag} + \underbrace{\frac{3}{4}\frac{C_L}{\rho_P^*}(\boldsymbol{u}_S^*\times\boldsymbol{\omega}_F^*)}_{Lift} \\ &+ \underbrace{\frac{1}{2\rho_P^*}\frac{D\boldsymbol{u}_F^*}{Dt^*}}_{Virtual\ Mass} \\ &+ \underbrace{\frac{1}{\rho_P^*}\frac{D\boldsymbol{u}_F^*}{Dt^*}}_{Pressure\ Gradient}.\end{aligned} \tag{5}$$

In Eqs. (4) and (5), $\boldsymbol{x}_P^*$ is the particle position vector, $\boldsymbol{u}_P^*$ the particle velocity vector, $\boldsymbol{u}_F^*$ the fluid velocity vector spectrally interpolated at the position of the particle, $\boldsymbol{u}_S^* = \boldsymbol{u}_F^* - \boldsymbol{u}_P^*$ the slip velocity between the fluid and the particle, d_P^* the particle diameter non-dimensionalised by the channel half-height, ρ_P^* the density ratio between the fluid and the particle and $\boldsymbol{\omega}_F^*$ the vorticity of the fluid interpolated spectrally at the particle position, given by $\boldsymbol{\omega}_F^* = \boldsymbol{\nabla}\times\boldsymbol{u}_F^*$. M_{VM} is the virtual mass modification term given by $M_{VM} = \left(1 + \frac{1}{2\rho_P^*}\right)$. The drag coefficient, C_D, is calculated dynamically using the correlations of Schiller and Naumann [13], where $C_D = 24f_D/Re_P$, with $f_D = (1 + 0.15Re_P^{0.687})$ when $Re_P > 0.5$ and $f_D = 24/Re_P$ otherwise (in the Stokes regime). Here, Re_P is the particle Reynolds number, given by $Re_P = Re_B d_P^*|\boldsymbol{u}_S^*|$. Further details on the calculation and origins of these terms are available in Mortimer et al. [18].

Particle translation during a time step is calculated after each fluid time step has completed. First, spectral interpolation is used to obtain the fluid velocity and its spatial derivatives at the particle positions. Then, Eqs. (4) and (5) are solved using a fourth-order Runge-Kutta scheme, with the time step equivalent to that of the fluid solver.

Collisions between particles and the channel walls are handled as elastic impacts, reversing the wall-normal component of the particle's velocity upon contact. In the periodic directions (streamwise and spanwise), particles exiting the domain on one

side are reintroduced at the corresponding position on the opposite side, maintaining the periodic nature of the channel flow. The training dataset consisted of 18 simulations, across two Reynolds numbers and multiple particle Stokes numbers based on shear scales, St^+, obtained by varying both the particle diameter and the particle-fluid density ratio. The fluid and particle properties used to train and validate are summarised in Table 1.

Table 1. Fluid and particle properties for each simulation considered. Simulation set names ending in T represent those used to train the ML algorithm, whereas V is used to indicate simulations performed for comparison purposes only

Parameter	SIM1T	SIM2V	SIM3T
Re_τ	180	240	300
ρ_P^*	2.5, 1111, 2041		
d_P^*	0.0025, 0.005, 0.0075		
St^+	0.028 → 574.03		
N_P	10,000		

2.3. Hybrid ANN Algorithm

Lagrangian trajectories obtained from the simulation methods described in Sections 2.1 and 2.2 are first pre-processed into a data array containing their vertical positions within the channel and corresponding velocity components, $y^*, u_{x,t}^*, u_{y,t}^*, u_{z,t}^*$. These are then combined with the simulation conditions and the velocities from the previous time step to form the complete input feature set as follows:

$$I = \begin{pmatrix} Re_\tau, \rho_P^*, d_P^*, y^*, \\ u_{x,t-1}^*, u_{y,t-1}^*, u_{y,t-1}^* \end{pmatrix}. \quad (5)$$

An artificial neural network was developed for this study due to its capacity to capture complex, non-linear relationships within the data and its proven accuracy in similar predictive modelling tasks. Previous studies have also demonstrated that ANNs can outperform other methods. The ANN model is configured with four hidden layers containing 256, 128, 64 and 32 configurable neurons and uses the rectified linear unit (*ReLU*) activation function. The number of layers and neurons, as well as the learning rate and batch size, were optimised beforehand through hyperparameter tuning.

Before training, the input features are normalized between 0 and 1 based on the minimum and maximum values of each variable. The training dataset consists of data from $N_P = 10{,}000$ particles with trajectories across 1000 instantaneous time states, sampled at intervals of $t^* = 0.005$. The impact of varying the number of trajectories used for training on the model's performance was evaluated and chosen to ensure optimal training root mean square error. The ANN was trained over 100 epochs and optimised using the adam optimiser, minimising the root-mean-square-error (RMSE) loss function, with a batch size of 32 and a train-test validation split of 0.3.

Once the model was adequately trained, synthetic particle trajectories are generated by first initialising each particle's position within the boundaries of the channel flow domain. The particles are then assigned velocities corresponding to the non-dimensional bulk velocity $U_B^* = 1.0$. During the hybrid ML-informed simulation, the ANN predicts the next particle velocity using the input feature set at the present time, as in Eq. (5). To account for local velocity fluctuations, a Gaussian noise model is also incorporated, defined as:

$$u_F'^* \sim N(\mu, \sigma^2), \quad (6)$$

where the mean, μ, and the standard deviation, σ, were chosen to validate against fluid flow predictions from DNS-LPT simulations and differ for each Reynolds number and parameter set. Furthermore, the wall-normal proximity, $|1 - y^*|$, is taken into account as an additional factor such that μ and σ are both functions of y^*. The predicted subsequent velocity may then be calculated using:

$$u_{p,t}^* = \bar{u}_P^* + u_F'^*, \quad (7)$$

where is $\bar{u}_P^*$ predicted by the trained ANN using the particle/fluid properties, previous velocities, and wall-normal positions within the channel. The particle positions are subsequently updated using a standard Euler time-stepping scheme using a time step identical to that employed in the DNS-LPT.

To handle particle-wall collisions, a collision detection and response mechanism is implemented, identical to that used in the LPT method. Specifically, in the vertical direction, the particle's velocity is reversed upon collision with the channel wall. In the streamwise and spanwise directions, particles exiting one boundary are reintroduced at the corresponding position on the opposite side, preserving the periodic flow characteristics of the channel.

3. RESULTS AND DISCUSSION

Initially, three simulations of unladen turbulent channel flows at SEM order $N = 7$ were conducted, using a constant pressure gradient driving force to establish a statistically stationary turbulence field for $Re_\tau = 180, 240$ and 300. The simulations were initialised with a condition featuring a mean velocity profile containing minor perturbations to promote the transition to turbulence. The simulations ran for $T_S^* = 100$ non-dimensional time units, with statistics collected during the final $50 \leq t^* \leq 100$. Additionally, statistics were measured at $t^* = 10$

intervals to ensure no temporal variations in the results. The $Re_\tau = 180$ and 300 single-phase channel flows have been validated in previous publications [18, 20].

To facilitate the Gaussian noise generation function, velocity fluctuation statistics were collected from the validated channel flows over new simulations with a temporal duration of $t^* = 100$. Figure 2 presents the probability density functions (p.d.f.s) for all three components of the velocity fluctuations, demonstrated in the $Re_\tau = 180$ simulation, and sampled from uniformly distributed locations throughout the channel domain over the entire simulation period. To validate the Gaussian noise model used for predicting local fluctuations on the particles, the sampled velocity fluctuations were compared against the model's predictions. In all three component directions, the noise model is shown to accurately capture the range and distribution of the fluctuating fluid velocities. Similar observations were made for the $Re_\tau = 240$ and 300 flows.

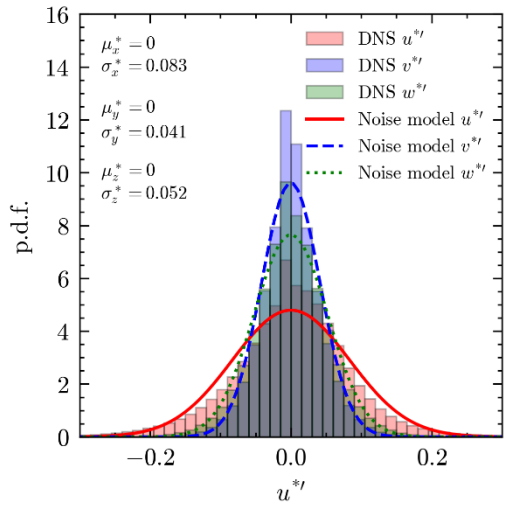

Figure 2: Gaussian noise model validation of velocity fluctuation components for single-phase DNS at $Re_\tau = 180$

In order to improve the accuracy of the Gaussian noise model when representing the true nature of velocity fluctuation distributions, the hybrid ML technique was enhanced to consider a wall proximity based standard deviation for the Gaussian profiles. Figure 3 demonstrates the functional relationship between wall distance and each component of the profile's standard deviation, σ. This was digitised as a look-up table, with points interpolated linearly between each measured region when calculating Eqs. (6) and (7). Because a major focus of the present work is to reduce runtimes while preserving DNS-like accuracy for particle trajectories, the resolution was chosen to resolve the important peaks. However, it should be noted that interpolation of the streamwise component may play a role in reducing accuracy in the hybrid ML model, since the actual peak is fairly sharp, and hence standard deviations are not as likely to be predicted with the same accuracy as in the bulk flow region.

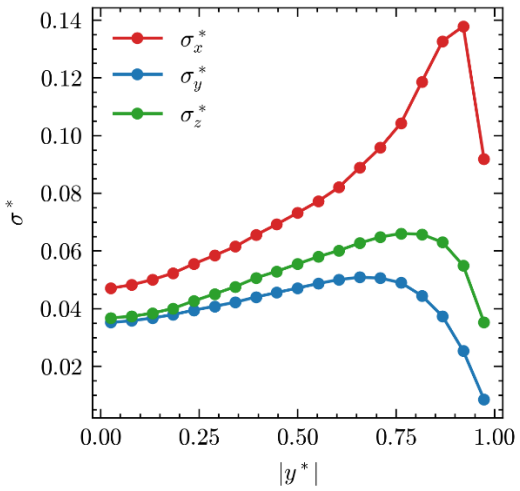

Figure 3: Gaussian noise standard deviation calculation based on velocity fluctuation components for single-phase DNS at $Re_\tau = 180$

The ANN was trained on 10,000 particle trajectories for each simulation dataset over 100 epochs. Training beyond this point led to overfitting, as indicated by an increase in RMSE for the validation dataset compared to the training dataset. After approximately 100 epochs, the validation MSE stabilised at around 4-5%. After training, the model was utilised to simulate particle-laden flows and the results were compared with those from DNS-LPT for corresponding simulations.

Figure 4 compares the predicted mean streamwise velocities of the hybrid ML particles with the DNS-LPT results for $Re_\tau = 180$ and $\rho_P^* = 2.5, d_P^* = 0.0025$. The predictions show excellent agreement across the wall-normal direction of the channel, with some slight overprediction in the bulk flow region. Similar comparisons for the RMS velocity fluctuations and the shear stress are shown in Fig. 5, revealing close alignment of the two predictions close to the wall but noticeable discrepancies in the channel's core. These deviations are more significant for the wall-normal and spanwise components. It is evident that the hybrid ML algorithm tends to overestimate the velocity fluctuations for these two components, likely due to the inability to fully capture emergent behaviour such as particle entrainment in low-speed streaks in the buffer layer, at which the accuracy is weakest. The algorithm also captures the general trends in the shear stress profile, though its accuracy is lower both within the buffer layer region as well as within the bulk flow region.

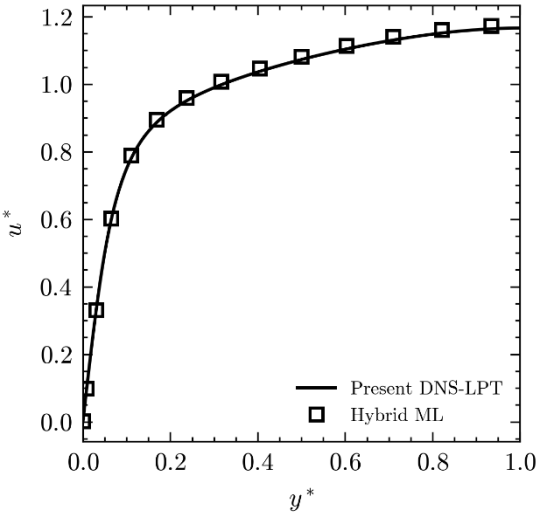

Figure 4: Comparison of mean particle streamwise velocity predictions between the present DNS results and the hybrid ML-predicted trajectories for $Re_\tau = 180$ and $\rho_P^* = 2.5, d_P^* = 0.0025$

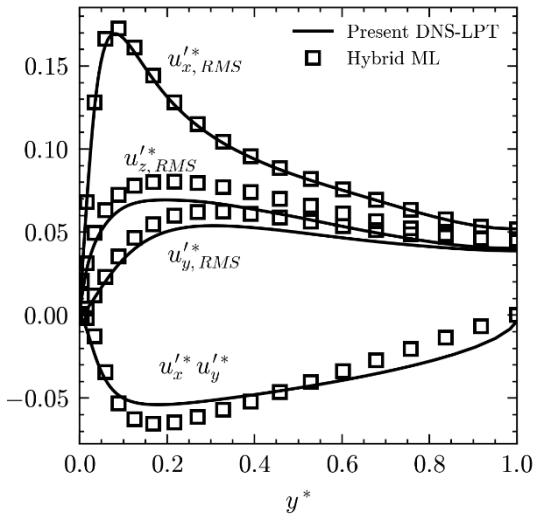

Figure 5: Comparison of and root-mean-square velocity fluctuations and shear stress predictions between the present DNS results and the hybrid ML-predicted trajectories for $Re_\tau = 180$ and $\rho_P^* = 2.5, d_P^* = 0.0025$

To determine the extent to which the hybrid ML algorithm can handle parameter sets outside those originally trained upon, an additional DNS-LPT simulation was performed at $Re_\tau = 240$, which lies halfway between those considered for the training datasets.

Figures 6 and 7 present the comparison of mean streamwise velocities and RMS velocity fluctuations for the untrained parameter set at $Re_\tau = 240$, in order to assess the generalisation capability of the hybrid ML model to conditions outside the training range.

In Figure 6, the predicted mean streamwise velocities show strong agreement with the DNS-LPT results across the wall-normal direction of the channel. Minor discrepancies are observed in the bulk region, where the ML model slightly overestimates the velocities. This overprediction could be attributed to the model's interpolation between the trained datasets at $Re_\tau = 180$ and 300, leading to a slight bias, though slight overprediction was observed in both training datasets. Nevertheless, the model accurately captures the overall trend, demonstrating its ability to generalise the mean particle behaviour to intermediate Reynolds numbers effectively.

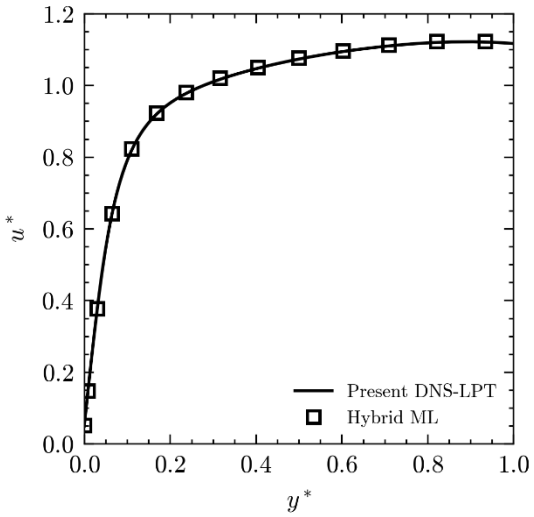

Figure 6: Comparison of mean particle streamwise velocity predictions between the present DNS results and the hybrid ML-predicted trajectories for $Re_\tau = 240$ and $\rho_P^* = 2.5, d_P^* = 0.0025$

Figure 7 compares the RMS velocity fluctuations, exhibiting strong agreement near the channel walls but noticeable deviations in the core region. These discrepancies are more pronounced for the wall-normal and spanwise components, consistent with observations for the other Reynolds numbers. The hybrid ML model tends to this time underpredict the fluctuations, particularly in regions where turbulence modulation is more significant. This is likely due to the model's inability to further fully capture complex emergent behaviours, such as particle clustering and low-speed streak entrainment, which are more prominent at higher Reynolds numbers.

Overall, the hybrid ML model exhibits strong predictive performance for an unseen Reynolds number, validating its generalisability across different flow conditions. However, the overestimation of velocity fluctuations indicates potential areas for improvement, such as incorporating additional physical models or enhancing Gaussian noise modelling techniques to

better inform the model of the presence of turbulent structures and particle-fluid interactions.

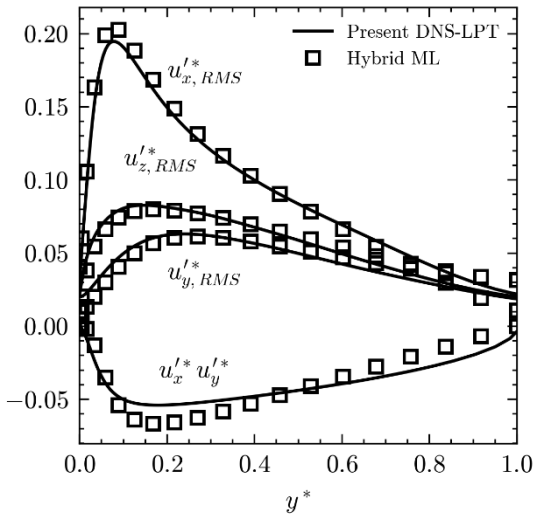

Figure 7: Comparison of and root-mean-square velocity fluctuations and shear stress predictions between the present DNS results and the hybrid ML-predicted trajectories for $Re_\tau = 240$ and $\rho_P^* = 2.5, d_P^* = 0.0025$

4. CONCLUSIONS

This study aimed to develop and validate an enhanced predictive model for simulating particle dispersion, advection, and wall interactions in turbulent channel flows using a hybrid machine learning algorithm. By utilising dynamic databases generated from DNS and LPT, another aim was to reduce the amount of simulation data required to achieve statistically stationary and accurate profiles while maintaining high prediction accuracy. Additionally, the model was tested on an unobserved parameter set at Re_τ=240 to evaluate its generalisability beyond the training parameter sets.

The results demonstrate that the hybrid ML algorithm, which incorporates an ANN model, effectively predicts particle trajectories with a significant reduction in computational cost. The model requires only around 10,000 DNS-LPT trajectories for training (c.f. 300,000 used in comparative studies [20]) and is able to generate additional ML-informed trajectories efficiently, resulting in substantial time and resource savings. This efficiency was particularly evident when generating synthetic trajectories for untrained Reynolds numbers, where the model captured the mean streamwise velocities with high accuracy. Although some discrepancies were noted in the RMS velocity fluctuations, particularly in the wall-normal and spanwise components, the overall agreement with DNS-LPT results was strong, validating the model's predictive capability.

The study demonstrates the potential of the hybrid ML algorithm for efficiently simulating particle dynamics in wall-bounded turbulent flows, making it a critical tool for real-time applications, such as digital twin technology. The model's ability to generalise to an unobserved Reynolds number showcases its robustness and adaptability across different flow conditions. However, the overestimation of velocity fluctuations in the channel core suggests areas for further refinement, such as enhancing the noise model or incorporating additional models (such as physics-informed components to the neural network) to better allow the training to understand interaction with complex flow structures.

Despite these areas for improvement, the reduced computational time and increased efficiency offered by this approach make it a promising alternative to traditional DNS-LPT simulations. Future work will focus on optimising the model architecture, exploring advanced noise modelling techniques, and extending its applicability to more complex flow scenarios and particle behaviours. These advancements will further enhance the model's accuracy and versatility, broadening its utility in both academic research and industrial applications, particularly where real-time analysis and decision-making are critical.

ACKNOWLEDGEMENTS

The authors are grateful to the UK Engineering and Physical Sciences Research Council for funding through the TRANSCEND (Transformative Science and Engineering for Nuclear Decommissioning) project (EP/S01019X/1), and Sellafield Ltd. for funding from the University of Leeds-Sellafield Ltd Centre of Expertise for Sludge (Particulates & Fluids).

REFERENCES

[1] Carleo, G., Cirac, I., Cranmer, K., Daudet, L., Schuld, M., Tishby, N., Vogt-Maranto, L., and Zdeborová, L., 2019, "Machine Learning and the Physical Sciences," *Reviews of Modern Physics*, Vol. 91, 045002.

[2] Mahesh, B., 2020, "Machine Learning Algorithms – A Review," *International Journal of Science and Research (IJSR)*, Vol. 9, pp. 381-386.

[3] Barragán-Montero, A., Javaid, U., Valdés, G., Nguyen, D., Desbordes, P., Macq, B., Willems, S., Vandewinckele, L., Holmström, M., Löfman, F., and Michiels, S., 2021, "Artificial Intelligence and Machine Learning for Medical Imaging: A Technology Review," *Physica Medica*, Vol. 83, pp. 242-256.

[4] Ali, A., Abd Razak, S., Othman, S.H., Eisa, T.A.E., Al-Dhaqm, A., Nasser, M., Elhassan, T., Elshafie, H., and Saif, A., 2012, "Financial Fraud Detection Based on Machine Learning:

A Systematic Literature Review," *Applied Sciences*, Vol. 12, 9637.

[5] Gupta, A., Anpalagan, A., Guan, L., and Khwaja, A.S., 2021, "Deep Learning for Object Detection and Scene Perception in Self-Driving Cars: Survey, Challenges, and Open Issues," *Array*, Vol. 10, 100057.

[6] Wang, Z., Xiao, D., Fang, F., Govindan, R., Pain, C.C., and Guo, Y., 2018, "Model Identification of Reduced Order Fluid Dynamics Systems Using Deep Learning," *International Journal for Numerical Methods in Fluids*, Vol. 86, pp. 255-268.

[7] de Oliveira Maionchi, D., Ainstein, L., dos Santos, F.P., and de Souza Júnior, M.B., 2022, "Computational Fluid Dynamics and Machine Learning as Tools for Optimization of Micromixers Geometry," *International Journal of Heat and Mass Transfer*, Vol. 194, 123110.

[8] Brunton, S.L., Noack, B.R., and Koumoutsakos, P., 2020, "Machine Learning for Fluid Mechanics," *Annual Review of Fluid Mechanics*, Vol. 52, pp. 477-508.

[9] Jain, P., Choudhury, A., Dutta, P., Kalita, K., and Barsocchi, P., 2021, "Random Forest Regression-Based Machine Learning Model for Accurate Estimation of Fluid Flow in Curved Pipes," *Processes*, Vol. 9, 2095.

[10] Li, K., Savari, C., Sheikh, H.A., and Barigou, M., 2023, "A Data-Driven Machine Learning Framework for Modeling of Turbulent Mixing Flows," *Physics of Fluids*, Vol. 35, 015150.

[11] Yang, Z., Li, K., and Barigou, M., 2023, "Experimentally Trained Hybrid Machine Learning Algorithm for Predicting Turbulent Particle-Laden Flows in Pipes," *Physics of Fluids*, Vol. 35, 113309.

[12] Benra, F.K., Dohmen, H.J., Pei, J., Schuster, S., and Wan, B., 2011, "A Comparison of One-Way and Two-Way Coupling Methods for Numerical Analysis of Fluid-Structure Interactions," *Journal of Applied Mathematics*, Vol. 2011, 853560.

[13] Mortimer, L.F., Njobuenwu, D.O., and Fairweather, M., 2020, "Agglomeration Dynamics in Liquid–Solid Particle-Laden Turbulent Channel Flows Using an Energy-Based Deterministic Approach," *Physics of Fluids*, Vol. 32, 043301.

[14] Wagg, D.J., Worden, K., Barthorpe, R.J., and Gardner, P., 2020, "Digital Twins: State-of-the-Art and Future Directions for Modeling and Simulation in Engineering Dynamics Applications," *ASCE-ASME Journal of Risk and Uncertainty in Engineering Systems, Part B: Mechanical Engineering*, Vol. 6, 030901.

[15] Fischer, P.F., Lottes, J.W., and Kerkemeier, S.G., "Nek5000," available at: http://nek5000.mcs.anl.gov/, accessed September 1, 2008.

[16] Maxey, M.R., 1987, "The Gravitational Settling of Aerosol Particles in Homogeneous Turbulence and Random Flow Fields," *Journal of Fluid Mechanics*, Vol. 174, pp. 441-465.

[17] Riley, J.J., and Patterson, J.R.G., 1974, "Diffusion Experiments with Numerically Integrated Isotropic Turbulence," *Physics of Fluids*, Vol. 17, pp. 292-297.

[18] Mortimer, L.F., Njobuenwu, D.O., and Fairweather, M., 2019, "Near-Wall Dynamics of Inertial Particles in Dilute Turbulent Channel Flows," *Physics of Fluids*, Vol. 31, 063302.

[19] Fairweather, M., and Hurn, J.P., 2008, "Validation of an Anisotropic Model of Turbulent Flows Containing Dispersed Solid Particles Applied to Gas-Solid Jets," *Computers and Chemical Engineering*, Vol. 32, pp. 590-599.

[20] Rupp, D.A., Mortimer, L.F., and Fairweather, M., 2023, "Stokes Number and Coupling Effects on Particle Interaction Behavior in Turbulent Channel Flows," *Physics of Fluids*, Vol. 35, 113307.